ELSEVIER

Journal of Organometallic Chemistry 637–639 (2001) 538–548

Journal of Organometallic Chemistry

www.elsevier.com/locate/jorganchem

Diferrocenyltriphosphines 2. Reversible phosphine deligation in the chemistry of diferrocenyltriphosphine Ru(II) dichloride complexes with nitriles and pyridines: towards a pH-switchable catalyst?

Ian R. Butler [a,*], Simon J. Coles [e], Marco Fontani [d], Michael B. Hursthouse [e], Eric Lewis [a], K.L.M. Abdul Malik [c], Marc Meunier [b], Piero Zanello [d]

[a] *Department of Chemistry, University of Wales, Bangor, Gwynedd LL57 2UW, UK*
[b] *Centre for Computational Chemistry, University of Wales, Bangor, Gwynedd LL57 2UW, UK*
[c] *Department of Chemistry, University of Wales, Cardiff, PO Box 912, Park Place, Cardiff CF10 3TB, UK*
[d] *Dipartimento di Chimica dell'Università di Siena, via Aldo Moro, 53100 Siena, Italy*
[e] *Department of Chemistry, University of Southampton, Highfield, Southampton SO17 1BJ, UK*

Received 2 February 2001; received in revised form 18 June 2001; accepted 20 June 2001

Abstract

The reaction of the complexes $[P_3\text{-}(P_3fc_2)RuCl_2]$, $P_3fc_2 = [\eta^5\text{-}(R_2PC_5H_4)Fe\text{-}\eta^5\text{:}\eta^5\text{-}(C_5H_4P(R')C_5H_4)Fe(\eta^5\text{-}C_5H_4PR_2)]$, R, R′ = Ph, iPr with linear nitriles results in the formation of the pseudooctahedral complexes, e.g. $[P_3\text{-}(P_3fc_2)Ru(NCCH_2R)Cl_2]$, R = H, Ph while the reaction of $[(P_3fc_2)RuCl_2]$ with pyridines results in partial deligation of one of the ferrocenyl phosphine ligand arms to give the products $[P_2\text{-}(\eta^5\text{-}(R_2PC_5H_4)Fe\text{-}\eta^5\text{:}\eta^5\text{-}(C_5H_4P(R')C_5H_4Fe(\eta^5\text{-}C_5H_4PR_2))Ru(pyr)_2Cl_2]$. The latter products revert to the starting complexes in the absence of excess pyridine in solution. The deligated pendant phosphine may be 'trapped' by reaction with Pd(II) or elemental sulfur. A molecular modelling study has been carried out to verify the conformations of the products. The single crystal structures of $mer\text{-}[P_3\text{-}(P_3fc)_2Ru(CO)Cl_2]$ and $mer\text{-}[P_2\text{-}(P_3fc)_2Ru(pyr)_2Cl_2]$ have been determined. Cyclic voltammetry supports the role assigned to pyridine in the reaction with the $P_3Fc_2\text{-}RuCl_2$ complexes. © 2001 Published by Elsevier Science B.V.

Keywords: Ferrocene; Phosphine ligand; Ruthenium complexes; Electrochemistry

1. Introduction

The design and synthesis of ligands for use in transition-metal catalysed processes is one of the most important areas of organometallic chemistry research. There is now an abundance of ligands available for use in such processes, so many in fact that it makes the selection of an optimum ligand for a particular reaction difficult for the practising organic chemist. It may be argued that it is no longer enough to concentrate resources on the synthesis of more ligands. This research is focussed on the design and synthesis of smart ligands, ligands that have interesting chemical and complexation behaviour. In a recent paper the synthesis of a number of triphosphinodiferrocenyl ligands of the type **1** (Fig. 1) was described [1]. These ligands may be obtained in high yields using a relatively simple synthetic methodology. The synthesis of Pd(II), Rh(I) and Ru(II) complexes of these ligands has also been documented [1,2].

The ruthenium complexes **2** (Fig. 1) are of special interest because of their similarity to some well known five co-ordinate complexes, such as $[Ru(triphos)Cl_2]$ [3], $triphos = [(Ph_2P(CH_2)_2)_2PPh]$ which exhibit interesting co-ordination and reaction chemistry. We were interested in developing the co-ordination chemistry of the new compounds, starting with simple addition reaction to the vacant pseudo octahedral site in the five co-ordinate complexes. One such addition, reported earlier by this research group, was the addition of carbon monoxide to the vacant site, which proceeds smoothly [2]

* Corresponding author. Fax: +44-1248-370-528.
E-mail address: i.r.butler@bangor.ac.uk, i.r.butler@ferrocene.com (I.R. Butler).

0022-328X/01/$ - see front matter © 2001 Published by Elsevier Science B.V.
PII: S0022-328X(01)01135-4

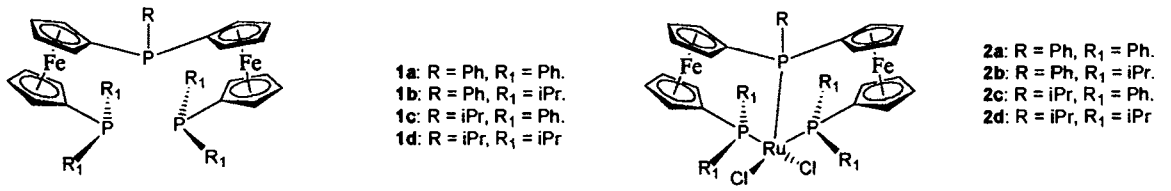

Fig. 1. Diferrocenyltriphosphines and their ruthenium complexes.

(Scheme 1a). The single crystal X-ray structure of one such compound is reported herein to clearly define the geometry of the carbonyl-containing products. The chemistry of the system in this case mimics that of [Ru(triphos)Cl_2]. It was decided to continue with this investigation to examine the use of nitriles and pyridines as potential ligands to complexes **2**.

2. Experimental

2.1. General experimental details

^{1}H-NMR and ^{31}P-NMR (relative to 85% phosphoric acid) spectra were recorded at 250 and 101 MHz, respectively using a Bruker WC-250 instrument. All other solvents used were predried using conventional methods and then were distilled prior to use. The complexes **2a**–**2b** were prepared according to the published procedure [2]. Materials and apparatus for the electrochemistry have been previously described [2]. Potential values are referred to the saturated calomel electrode (SCE). Under the present experimental conditions the one-electron oxidation of ferrocene occurs at $E° = +0.39$ V. Compound **3c** was prepared as previously described [2] and it was crystallised by slow diffusion of a chloroform/petrol layered mixture. The visible spectra of complexes **2a**–**2d** were obtained by standard methods: UV: λ_{max} (nm) values **2a**, 484, **2b**, 508, **2c**, 488, **2d**, 504 (CH_2Cl_2). Molecular modelling was carried out using the Molecular Simulations Inc. Suite of Programs. Dynamics calculations were performed using the DISCOVER® program.

2.2. X-ray crystallography for [$(P_3fc)_2$Ru(CO)Cl_2] (3c)

The crystal used for X-ray work was obtained by slow diffusion of a $CHCl_3$–hexane mixture. All measurements were made on a Delft Instruments FAST area detector diffractometer positioned at the window of a rotating anode generator with Mo–K_α radiation by following procedures described earlier [4].

2.2.1. Crystal data

Formula $C_{48}H_{42}Cl_2Fe_2OP_3Ru$, $2CHCl_3$, F_W 1250.13, monoclinic, space group $P2_1/n$ (no. 14), $a = 19.818(4)$, $b = 11.977(2)$, $c = 21.558(4)$ Å, $\beta = 98.79(3)°$, $U = 5057(2)$ Å^3 (least-squares refinement of diffractometer angles for 250 reflections within $1.91 \leq \theta \leq 25.07°$), $Z = 4$, $D_{calc} = 1.642$ Mg m^{-3}, μ(Mo–K_α) = 1.417 mm^{-1}, $F(000) = 2516$, crystal size = $0.26 \times 0.18 \times 0.15$ mm^3, $T = 150(2)$ K. Intensities of 18447 reflections

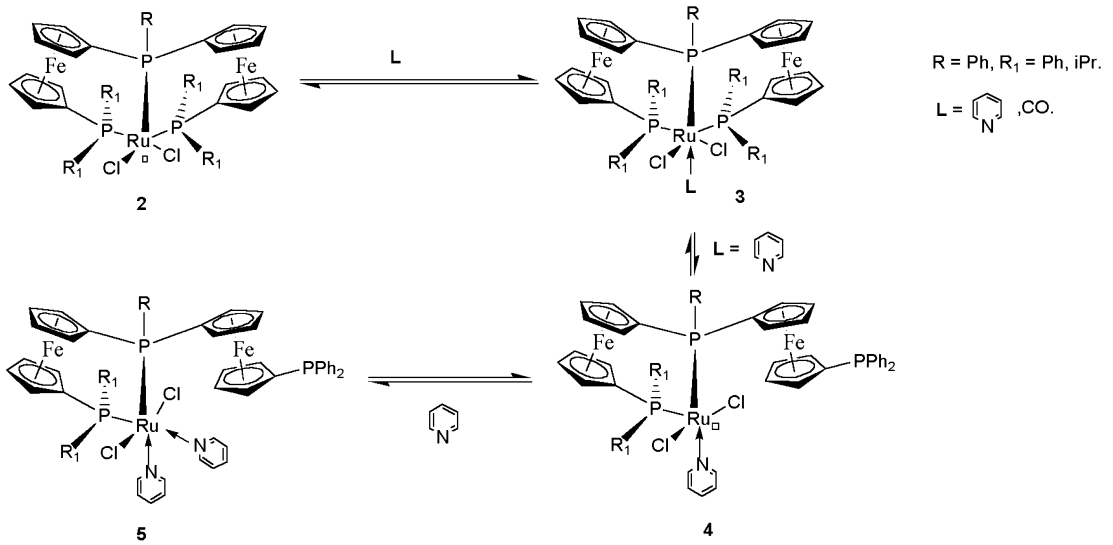

Scheme 1. The binding of CO to the five-coordinate complex and pyridine coordination which triggers the deligation of a phosphine ligand.

Table 1
Selected bond lengths (Å) and bond angles (°) for $[(P_3fc)_2Ru(CO)Cl_2]$ (**3c**)

Bond lengths			
Ru(1)–P(1)	2.438(3)	Ru(1)–P(2)	2.529(3)
Ru(1)–P(3)	2.404(3)	Ru(1)–Cl(1)	2.427(3)
Ru(1)–Cl(2)	2.436(3)	Ru(1)–C(1)	1.947(14)
Fe(1)–C(5)	1.997(11)	Fe(1)–C(3)	2.005(11)
Fe(1)–C(6)	2.015(11)	Fe(1)–C(4)	2.022(11)
Fe(1)–C(7)	2.023(11)	Fe(1)–C(11)	2.026(10)
Fe(1)–C(10)	2.029(11)	Fe(1)–C(9)	2.039(11)
Fe(1)–C(8)	2.053(12)	Fe(1)–C(2)	2.082(11)
Fe(2)–C(18)	1.992(11)	Fe(2)–C(19)	1.995(11)
Fe(2)–C(12)	1.996(11)	Fe(2)–C(17)	2.015(11)
Fe(2)–C(16)	2.016(11)	Fe(2)–C(15)	2.029(11)
Fe(2)–C(20)	2.042(11)	Fe(2)–C(21)	2.061(11)
Fe(2)–C(14)	2.063(12)	Fe(2)–C(13)	2.071(11)
Bond angles			
C(1)–Ru(1)–P(3)	85.7(4)	C(1)–Ru(1)–Cl(1)	98.3(5)
P(3)–Ru(1)–Cl(1)	82.74(11)	C(1)–Ru(1)–Cl(2)	84.3(4)
P(3)–Ru(1)–Cl(2)	89.18(11)	Cl(1)–Ru(1)–Cl(2)	171.29(10)
C(1)–Ru(1)–P(1)	85.5(4)	P(3)–Ru(1)–P(1)	162.16(11)
Cl(1)–Ru(1)–P(1)	83.24(10)	Cl(2)–Ru(1)–P(1)	105.30(10)
C(1)–Ru(1)–P(2)	166.4(5)	P(3)–Ru(1)–P(2)	99.72(11)
Cl(1)–Ru(1)–P(2)	94.78(11)	Cl(2)–Ru(1)–P(2)	83.35(11)
P(1)–Ru(1)–P(2)	92.39(10)		

Table 2
Selected bond lengths (Å) and bond angles (°) for $[P_2$-$(P_3fc)_2Ru(pyr)_2Cl_2]$ (**5a**)

Bond lengths			
N1–Ru1	2.170(2)	N2–Ru1	2.175(2)
P1–Ru1	2.3076(9)	P2–Ru1	2.3312(11)
Ru1–Cl2	2.4203(11)	Ru1–Cl1	2.4224(10)
C23–Fe1	2.020(3)	C24–Fe1	2.027(3)
C25–Fe1	2.045(3)	C26–Fe1	2.044(3)
C27–Fe1	2.032(3)	C28–Fe1	2.023(3)
C29–Fe1	2.039(3)	C30–Fe1	2.037(3)
C31–Fe1	2.038(3)	C32–Fe1	2.053(3)
C39–Fe2	2.062(3)	C40–Fe2	2.048(3)
C41–Fe2	2.044(3)	C42–Fe2	2.050(3)
C43–Fe2	2.048(3)	C44–Fe2	2.051(3)
C45–Fe2	2.066(3)	C46–Fe2	2.052(3)
C47–Fe2	2.029(3)	C48–Fe2	2.038(3)
Bond angles			
N1–Ru1–N2	83.25(9)	N1–Ru1–P1	91.87(7)
N2–Ru1–P1	173.30(6)	N1–Ru1–P2	169.23(6)
N2–Ru1–P2	90.53(7)	P1–Ru1–P2	94.97(4)
N1–Ru1–Cl2	86.20(7)	N2–Ru1–Cl2	87.78(7)
P1–Ru1–Cl2	87.31(4)	P2–Ru1–Cl2	102.40(4)
N1–Ru1–Cl1	85.20(7)	N2–Ru1–Cl1	88.15(7)
P1–Ru1–Cl1	96.05(4)	P2–Ru1–Cl1	85.82(4)
Cl2–Ru1–Cl1	170.86(3)		

$[1.91 \leq \theta \leq 25.07°;\ -23 \leq h \leq 23,\ -9 \leq k \leq 14,\ -25 \leq l \leq 25]$ were recorded and processed to obtain 7395 $[R_{int} = 0.1307]$ unique data with $I > 2\sigma(I)$. The data were corrected for absorption effects (DIFABS) [5] (min. and max. absorption correction factors 0.836, 1.018).

The structure was solved by direct methods (SHELXS-86) [6] and refined by full-matrix least-squares on F^2 using all unique data with intensities greater than 0 (SHELXL-93) [7]. The non-hydrogen atoms were all anisotropic. There were two molecules of $CHCl_3$ solvate (per complex) with some of the chlorine positions partially occupied. The atoms C(1), C(49), C(50) Cl(3)–Cl(11) were refined with ISOR = 0.01 to prevent them becoming 'non-positive-definite'. The C–Cl distances in the solvates were also refined with the constraint 1.76 Å. The H atoms of $CHCl_3$ were ignored; other H atoms were included in calculated positions (riding model) with $U_{iso} = 1.2 \times U_{eq}$ of the parent carbon. Final R {on 2067 data with $I > 2\sigma(I)$} = 0.0524 and wR_2 (on F^2, all 7395 data) = 0.1168, $w = 1/[\sigma^2(F_o^2)]$. Selected bond lengths and angles are given in Table 1.

2.3. X-ray crystallography for $[P_2$-$(P_3fc)_2Ru(pyr)_2Cl_2]$ (**5b**)

Data were measured on a Nonius KappaCCD area detector equipped with a rotating anode generator (Mo–K_α radiation) and controlled by COLLECT [8] software.

2.3.1. Crystal data

Formula $C_{60}H_{51}Cl_2Fe_2N_2P_3Ru$, $3C_3H_6O$, F_W 1350.84, triclinic, space group $P\bar{1}$, $a = 11.927(2)$, $b = 15.891(3)$, $c = 17.912(4)$ Å, $\alpha = 111.29(3)$, $\beta = 92.55(3)$, $\gamma = 101.54(3)°$, $U = 3073.7(11)$ Å^3, $Z = 2$, $D_{calc} = 1.460$ Mg m^{-3}, μ(Mo–K_α) = 0.923 mm^{-1}, $F(000) = 1392$, crystal size = 0.16 × 0.14 × 0.06 mm^3, $T = 150(2)$ K. Intensities of 45139 reflections $[2.92 \leq \theta \leq 27.5°;\ -15 \leq h \leq 15,\ -20 \leq k \leq 20,\ -23 \leq l \leq 23]$ were recorded and processed to obtain 13818 $[R_{int} = 0.0967]$ unique data with $I > 2\sigma(I)$. The data were corrected for absorption effects (SORTAV) [9] (min. and max. transmission factors 0.8664, 0.9467). The structure was solved by direct methods and refined by full-matrix least-squares on F^2 using all unique data using the SHELX-97 suite of programs [10]. The non-hydrogen atoms were all anisotropic. There were three molecules of C_3H_6O solvate per complex molecule. H atoms were included in calculated positions (riding model) with $U_{iso} = 1.2 \times U_{eq}$ of the parent carbon. Final R {on 10096 data with $I > 2\sigma(I)$} = 0.0428 and wR_2 (on F^2, all 13818 data) = 0.1076, $w = 1/[\sigma^2(F_o^2)]$. Selected bond lengths and angles are given in Table 2.

2.4. NMR reactions: general procedure

A solution of complex **2b** (500 mg, 0.57 mmol) in *d*-chloroform (15 cm^3) was used as a standard. The solution was subdivided into 1.5 cm^3 fractions and to each a tenfold excess of the appropriate ligand was added. The ^{1}H- and ^{31}P-NMR spectra were recorded.

Table 3
Co-ordination ^{31}P-NMR chemical shifts on addition of ligands to complex **2b** to form new complexes of the general type **3b**

Ligand	$PiPr_2$(*cis*)	PPh(*trans*)	$\Delta PiPr_2$	ΔPPh
CO [≠]	21.13	−20.59	+37.7	+102.8
CH_3CN	21.96	27.32	+15.6	+54.9
$PhCH_2CN$	22.77	28.17	+14.8	+54.1
$N(CH_2CH_2OH)_3$	46.38	55.33	−8.84	+26.9

2.5. Isolation of pyridine complexes *5a*, *5b* (general procedure)

A solution of the complex (50 mg, 0.049 mmol), **2a** or (50 mg, 0.057mmol) **2b** in dichloromethane (3cm^3) was treated with the appropriate pyridine base (10–30-fold molar excess). The solution turned yellow or orange from the initial violet colour. *n*-Hexane was added dropwise until the solution became turbid. The mixture was filtered and the solution was cooled to −20 °C for 10 h. The product, in each case, crystallises from solution as yellow or orange/yellow nodules. N.B.: resolution in CH_2Cl_2 results in partial reconversion to **2a** or **2b**, respectively. Spectroscopic data are presented in Tables 3 and 4.

5b: ^{1}H-NMR ($CDCl_3$): 0.36 (dd, 3H, $J_{P-H} = 7$, 12 Hz), 0.51(dd, $J_{P-H} = 7$, 12 Hz, 3H), 0.58–0.79 (series of overlapping dd's, 12H), 1.18–1.33 (2 overlapping dd's, $J_S = 7$ Hz, 13 Hz, 6H), 2.07 (br m, 2H), 2.66 (br m, 2H), aliphatic protons; 2.12 (m, 1H), 3.12 (m, 1H), 3.17 (m, 1H), 3.22 (m, 1H), 3.47 (m, 1H), 3.57 (m, 1H), 3.66 (m, 1H), 3.92 (m, 1H), 4.07 (m, 1H), 4.16 (m, 1H), 4.22 (m, 1H), 4.25 (m, 1H), 4.40 (m, 1H), 4.90 (m, 1H), 5.13 (m, 1H), 5.17 (m, 1H), ferrocenyl protons; 7.02–7.20 (ms, 5H). ^{31}P-NMR: −1.13(s), +30.85 (d, $J = 35$ Hz), +44.61 (d, $J = 35$ Hz). Anal. Calc. for $C_{48}H_{59}Cl_2Fe_2N_2P_3Ru$: C, 55.36; H, 5.71; N, 2.69. Found: C, 55.50; H, 5.53; N, 2.53% (as dried, non-crystalline powder). Mass spectrum: no parent ion (1038–44 amu) was observed, EI, CI or FAB. Crystals suitable for X-ray diffraction were grown in acetone.

Complex **5b** + $Pd(COD)Cl_2$: ^{1}H-NMR($CDCl_3$): 0.41 (dd, $J = 7$ Hz, 12 Hz, 3H), 0.57 (dd, $J = 7$ Hz, 12 Hz, 3H), 1.03–1.38 (overlapping dd's, 18H), 2.35 (m, 2H), 2.82 (m, 2H), aliphatic protons, 3.20 (m, H), 3.64 (m, 1H), 3.94 (m, 1H), 4.02 (m, 1H), 4.17 (m, 1H), 4.26 (m, 1H), 4.33 (m, 1H), 4.50 (m, 1H), 5.03 (m, 1H), 5.23 (m, 1H), other multiplets are overlapped; ferrocenyl protons; 7.27–7.51 (br m, 5H) (aromatic protons), 7.13 (m, 2H), 7.52 (m, 2H), 8.50 (m, 2H), 8.72 (m, 2H). ^{31}P-NMR: +23.90 (s), +30.79, (br d), +44.69 (d).

5a: ^{1}H-NMR ($CDCl_3$): 2.29 (m, 1H), 2.92 (m, 1H), 3.19 (m, 1H), 3.39 (m, 1H), 3.45 (m, 1H), 3.46 (m, 1H), 3.61 (m, 1H), 3.70 (m, 1H), 3.79 (m, 1H), 3.99 (m, 1H), 4.29 (m, 1H), 4.37 (m, 1H), 4.47 (m, 1H), 5.00 (m, 1H), 5.80 (m, 1H), ferrocenyl protons; 6.70–7.00 (br m, 4H), 7.06–7.50 (m's, 21H), (phenyl protons) 8.47 (br s), 8.80 (br s), pyridinyl protons; ^{31}P-NMR ($CDCl_3$): −18.71 (s), +32.41 (d), +50. 67 (d) $J_{P-P} = 36.6$ Hz (**2a**, +90.84 (t), +38.30 (d), $J_{P-P} = 30.5$ Hz). Anal. Calc. for $C_{60}H_{51}Cl_2Fe_2N_2P_3Ru$: C, 61.20; H, 4.37; N, 2.38. Found: C, 60.78; H, 4.32; N, 2.25 (as dry, non solvated, powder). Crystals may be grown in acetone.

2.5.1. Reaction with [Pd(COD)Cl$_2$]

[5a $PdCl_2$]: ^{1}H-NMR ($CDCl_3$, d^5-pyr) 2.66 (m, 1H), 3.00 (m, 1H), 3.45 (m, 1H), 3.92 (m, 1H), 3.95 (m, 1H), 4.04 (m, 1), 4.12 (m, 1H), 4.37 (m, 1H), 4.43 (2m, 2H), 4.50 (m, 1H), 4.60 (m, 1H), 4.68 (m, H), 5.30 (m, 1H), 5.35 (m, 1H), 5.90 (m, 1H), 5.53 (traces of COD). 6.50–7.75 (series of overlapping multiplets, 25H). ^{31}P-

Table 4
Reaction of Complex **2b** with pyridines and related ligands: ^{31}P-NMR Chemical Shift Values

Ligand (pK_a)	PPh	$PiPr_A$	$PiPr_B$	ΔPPh	$\Delta PiPr_c$
Pyridine (5.25)	30.85	44.61	−1.13	+51.4	−6.9
2-Methylpyridine (5.97) (α-picoline)	No reaction at ambient temperature				
3-Methylpyridine (5.68) (β-picoline)	30.45	44.10	−0.85	+51.8	−6.6
4-Methylpyridine (6.02) (γ-picoline)	30.44	44.54	−0.84	+51.8	−7.0
3-Acetylpyridine	30.16	45.27	−1.21	+52.10	−7.7
4,4′-Dipyridine	29.70	44.35	−1.10	+52.53	−6.8
Pyridazine (2.24)	31.66	48.68	−1.85	+50.60	−9.1
Pyrazine (0.65)	28.60	44.10	−1.29	+53.85	−6.5
Pyrazole	33.08	49.11	−0.99	+49.20	−10.2
Isoquinoline (5.42)	30.18	44.53	−1.08	+52.10	−7.0
Quinoline (4.90), diphenylacetylene, quinoxaline (0.56), pyrrole, 3-methylisoquinoline	No reaction [≠]				
Partial delegation					
Acetonitrile	34.90	51.78	−1.16	+47.3	−14.5
2,2′-dipyridine	28.50	35.60	−1.16	+53.7	−1.6
D+α-*N*,*N*-dimethylphenylethylamine	28.09	51.66	−1.39	+54.2	−14.4
Benzylnitrile	23.50	31.88	−1.39	+58.7	+5.4

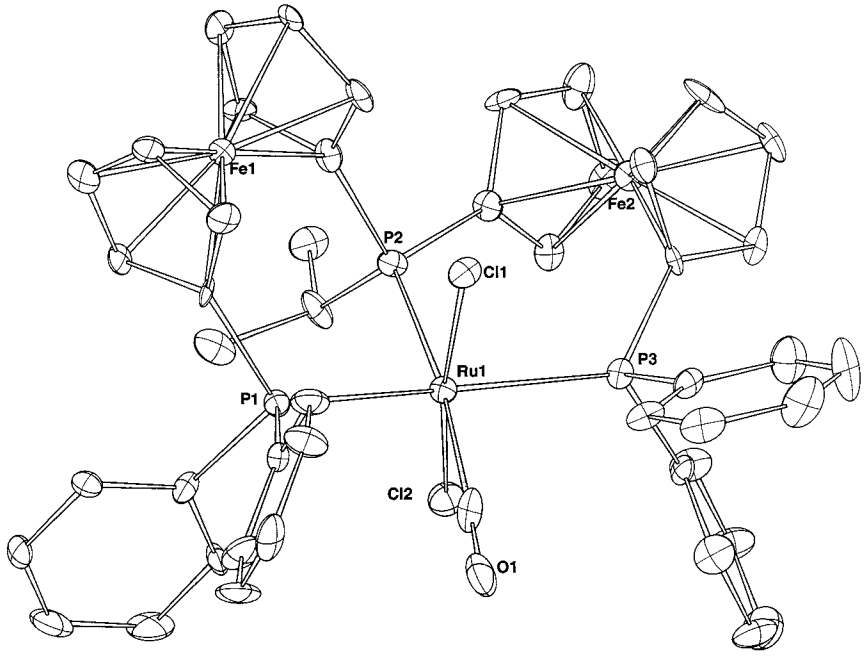

Fig. 2. The single crystal structure of compound **3c** [18].

NMR: +23.24 (s), +32.41 (d), +50.73 (d), J_{P-P} = 36.6 Hz.

2.6. Reaction of compound **2a** with elemental sulfur

A mixture of compound **5a** was prepared as described above on a 1 g scale in dichloromethane to which elemental sulfur 250 mg was added. The solution was filtered and layered with hexane. The golden yellow/tan crystals of the product, which were obtained after 24 h slow diffusion, were isolated and washed with petrol. **7a**: ^{1}H-NMR ($CDCl_3$, d^5-pyr): 2.31 (bs, 1H), 3.06 (bs, 1H), 3.59 (bs, 1H), 3.76 (bs, 1H), 3.90 (bs, 1H), 3.93 (bs, 1H), 3.96 (bm's 2H), 4.17 (bs, 1H), 4.24 (bs, 1H), 4.46 (bs, 1H), 4.51 (bs, 1H), 4.62 (bs, 1H), 5.08 (bs, 1H), 5.30 (bs, 1H), 5.89 (bs, 1H), (ferrocenyls). 6.40–7.70 (series of overlapping multiplets, 36H), 8.20, (bm, 1H), 8.31 (bm, 1H), 8.82, (bm, 2H) 9.18 (bm, 1H).). ^{31}P-NMR: +32.71 (br s), +40.91(s), +50.67 (br s). Anal. Calc. for $C_{60}H_{51}Cl_2Fe_2N_2P_3RuS.CH_2Cl_2$: C, 56.64; H, 4.13; N, 2.17. Found: C, 56.78; H, 4.19; N, 2.25%.

3. Results and discussion

In a recent paper the synthesis of a series of Ru(II) complexes of the diferrocenyltriphosphine ligands **1** was described. These complexes react with carbon monoxide rapidly at 25 °C to form the pseudo octahedral product complexes **3**, (Scheme 1). In the initial investigation only powdered microcrystalline samples of **3** were obtained however using a revised isolation procedure we have now been able to isolate crystalline samples. The single crystal structure of one of these products, **3c**, has been determined. The reaction chemistry in this case is analogous to that of [Ru(triphos)Cl_2], triphos = $[Ph_2(CH_2)_2]_2PPh$ [3]. A correlation may be drawn between the ^{31}P chemical shifts of the ligand phosphorus resonances with the carbonyl stretching frequencies for these complexes. Thus, as expected, the more basic phosphine ligands have the effect of increasing the strength of the metal–carbonyl bond. For example the carbonyl stretching frequencies of these complexes **3a**–**3d** are observed at 1988, 1962, 1974 and 1954 cm^{-1}, respectively, indicating that the stronger metal carbonyl bonding occurs when more electron density is provided by the ferrocenylphosphine ligands. The ^{31}P-NMR chemical shifts for the phosphine *trans* to the carbonyl group in complexes **3a**–**3d** are respectively are at −8.7, −20.6, +18.05 and +2.77 ppm [2].

3.1. X-ray structure of [$(P_3fc)_2Ru(CO)Cl_2$] (**3c**)

The molecular structure of (**3c**) is shown in Fig. 2, which also indicates the crystallographic atom numbering scheme used for the non-carbon atoms. The disordered solvate species ($CHCl_3$) in the lattice are omitted for clarity. Selected molecular geometry parameters are presented in Table 1.

There are numerous reports on the structures of metal complexes containing PPP donor ligands [11–17], but complexes of tridentate *PPP* ligand with two ferro-

cenyl units are relatively rare, the only such example, $[RuCl_2\{Ph_2P(C_5H_4)_2Fe\}_2P(Ph)]\cdot 2CHCl_3$, (**2a**), being reported very recently [2]. This compound was shown to have a five co-ordinate square-pyramidal geometry with the bridging phosphorus at the apical position, and a phenyl hydrogen blocking the vacant 'sixth' co-ordination site on the Ru atom. The present structure is very similar, with a carbonyl group occupying the 'sixth' co-ordination site and thus completing the typical six co-ordinate octahedral geometry around the metal atom. The main deviations from ideal geometry are the angles (a) P(1)–Ru(1)–Cl(2) which, instead of being ca. 90°, has a value of 105.30(10)°, and (b) P(1)–Ru(1)–P(3) and P(2)–Ru(1)–Cl(1) which, instead of 180°, are 162.16(11) and 166.4(5)°, respectively. The Cl(1)–Ru(1)–Cl(2) angle is close to linear [171.29(10)°], and shows less distortion compared with **2a** [153.19(4)°]. The much wider P(1)–Ru(1)–Cl(2) angle may be explained by the short Cl(2)···H(26) 2.521 Å steric interaction.

3.2. Co-ordination studies

It was of interest to examine the possibility of using the pseudo five co-ordinate complexes **2** as a means of obtaining a scale of ligand basicity, i.e. to react the complexes with a range of related ligands to use the ^{31}P-NMR shifts as a basis for a correlation. The colour change (violet to yellow), on going from five to six co-ordination, provides a rapid visual measure. The first complex chosen to be examined was complex **2b** because of its high solubility in a range of solvents. The reactions were investigated using ^{31}P-NMR using the ligand chemical shifts as a means of correlation. The reaction of complex **2b** in acetonitrile was first considered.

There was a considerable upfield shift in the ligand resonances observed on addition of acetonitrile to a $CDCl_3$ solution of complex **2b**. The solution changed colour from violet to yellow as expected. The ^{31}P ligand resonances are observed at $+82.23$ and $+37.54$ ppm, respectively, in compound **2b**, the latter being due to the two equivalent isopropyl substituted phosphorus nuclei while in the product complex the new resonances were observed at $+27.32$ and $+21.96$ ppm, respectively. The larger upfield shift ($+54.9$ ppm) is observed for the phosphorus *trans* to the incoming acetonitrile ligand. This chemical shift is considerably smaller than that previously observed in the case of carbon monoxide co-ordination ($+102.8$) an indication of its weaker ligand field strength (i.e. lack of back donation). More interestingly, however, was the observation that the reaction is not clean in that three other weaker resonances were also observed at chemical shift values of $+51.78$, $+34.90$ and -1.57 ppm, respectively, the former two resonances being doublets and the latter a singlet. The position and multiplicity of the latter resonances is indicative of deligation of a phosphine group. An identical observation was made in the reaction of complex **2b** with phenylacetonitrile, under identical experimental conditions. The data are summarised in Table 3 and in part in Table 4. Interestingly in the case of triethanolamine the terminal phosphorus resonances are shifted upfield, i.e. stronger bonding or a marked change in geometry is indicated, possibly due to an interaction with the hydroxy group(s).

The next stage of the investigation progressed to examine the co-ordination behaviour of pyridine. When the ^{31}P-NMR spectrum was examined it was clear that in this case one of the terminal isopropyl-substituted phosphines had become detached from the metal centre i.e. deligated, however it was not clear if the product complex was a mono or bis-pyridinyl complex. It could be envisaged that the pyridine entered the 'vacant' co-ordination site, which subsequently triggered the deligation of the geometrically strained phosphine. The free site could then be filled by a second pyridine, (Scheme 1b).

To extend the scope of the coordination study and to continue with the original objective it was decided to examine the co-ordination behaviour of a number of substituted pyridines and related ligands. Of these ligands pyrazine, pyradazine, 3-acetylpyridine and *iso*-quinoline reacted in an analogous fashion to pyridine while quinoline, quinoxaline, 3-methyl-*iso*-quinoline, pyrrole and 1,2-diphenylacetylene did not react at ambient temperature (although several of these ligands did show evidence of reaction after standing for 20 h). It is clear that the steric constraints inhibited the co-ordination of 2-methylpyridine, quinoline, 2,2′-dipyridine and quinoxaline. The relevant data are summarised in Table 4.

At this point it was clearly evident from the spectroscopic data that (i.e. the similarity of the phosphorus chemical shift data) it would be impossible to use the coordination reaction as a means of obtaining a ligand basicity scale because of the electronic buffering effect of the metal–ligand interaction. However more interesting, as a potential pH trigger, was the pyridine-assisted metal–phosphine cleavage reaction, which may be able to be useful in a switchable catalysis regime. Thus this reaction was explored in more detail. To this point only ^{31}P data have been analysed therefore it became evident that ^{1}H-NMR data were also required. A *d*-chloroform solution of complex **2a** or **2b** was treated with a drop of pyridine to obtain the yellow solution. The solvent was then removed under vacuum to leave a yellow oil, which was hexane washed. The product was redissolved in *d*-chloroform whereupon the violet colour was partially re-established demonstrating the reversibility of the reaction. The ^{1}H-NMR

spectrum obtained was that of a mixture of the starting compound and a pyridine-containing complex presumed to be the product. No evidence for the formation of any intermediate complex was observed, i.e. no evidence for the 5-coordinate complex. A pure sample of the yellow product complex **3a** was however obtained on cooling the original hexane washings to yield yellow nodules. The yellow product was redissolved in *d*-chloroform and the ^{1}H-NMR was re-recorded. Again the starting complex was regenerated and the pyridine was liberated to solution. Integration of the pyridine resonances indicates the present of two pyridine molecules per complex.

A solution of **2b** in $CDCl_3$ was treated with one drop of 4-methylpyridine to effect delegation then a $CDCl_3$ solution containing [Pd(1,5-COD)Cl_2] was added dropwise. It was evident from the results obtained that the pendant phosphine was co-ordinated to the palladium centre; the free phosphine resonance shifted downfield to +42.37 ppm from −0.84 ppm while the remaining resonances shifted only slightly from +30.44 to +30.62 ppm and from +44.54 to +44.48 ppm, respectively.

The product complex **6b** is red in contrast to the yellow **5b**. A similar result was observed for the pyridine complex **5b**. Although it was possible to isolate samples of **6b** directly by precipitation on attempted recrystallisation partial decomposition occurred and it was not possible to obtain a sample for crystallographic analysis. The ^{1}H-NMR spectrum of such samples, indicate that the reaction is not clean, hence the difficulty on obtaining a crystalline sample. This is despite apparently clean ^{31}P-NMR spectra, e.g. Fig. 3C.

Finally another method available for trapping the deligated complexes was to add sulfur to the solution obtained on pyridine addition. Compound **2a** in a range of solvents may be thus trapped to provide crystalline samples of the complex **7a**. The pendant phosphine sulfide shifts to lower field than than that of the metal-bound phosphine. This can be seen in Fig. 3D.

The phosphine, which is unbound is thus oxidised and is not able to reco-ordinate on removal of pyridine. This complex should be able to react with a range of bidentate ligand to displace the pyridine groups and thus extend the synthetic possibilities. This, in part, will be the subject of the next paper in this series.

Returning to the quest for absolute structural information regarding compounds **5a** and **5b**, it was subsequently found it was possible to crystallise compound **5a**, which is slightly less soluble in organic solvents. Crystals could be obtained from dichloromethane–hexane solutions or from acetone. A crystal of the product **5a**, which was obtained from acetone, was subjected to single crystal X-ray diffraction and the results are discussed below.

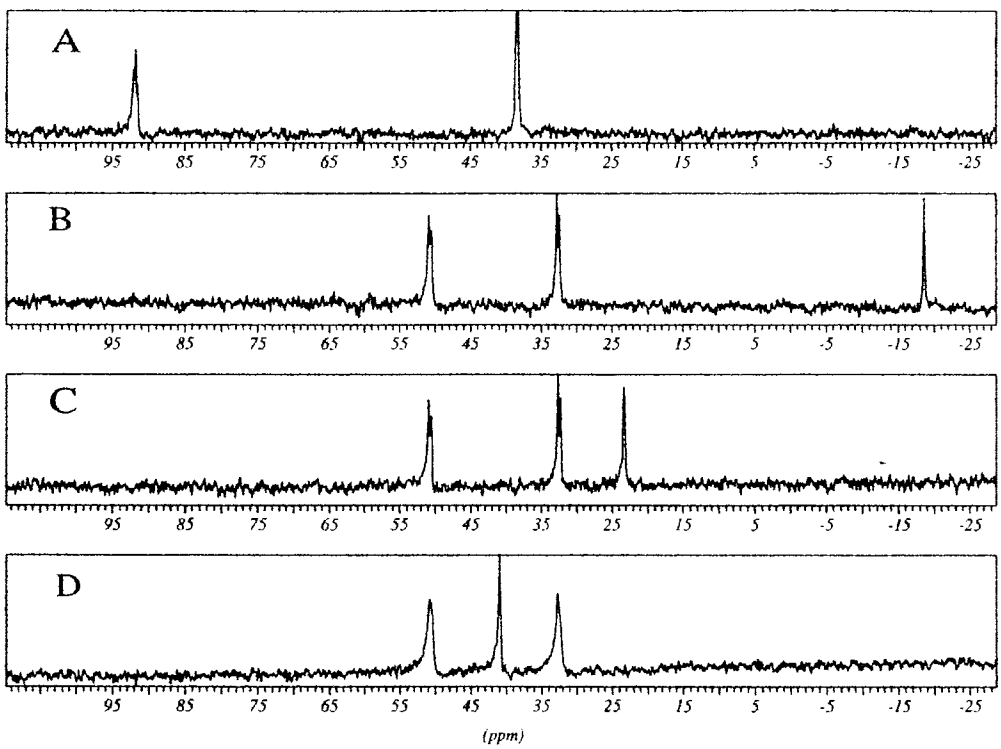

Fig. 3. The ^{31}P-NMR spectra of (A) complex **2a**, (B) complex after addition of pyridine-formation of **5a**, (C) the complex after addition of Pd(COD)Cl_2 and (D) after the addition of excess elemental sulfur (formation of **7a**).

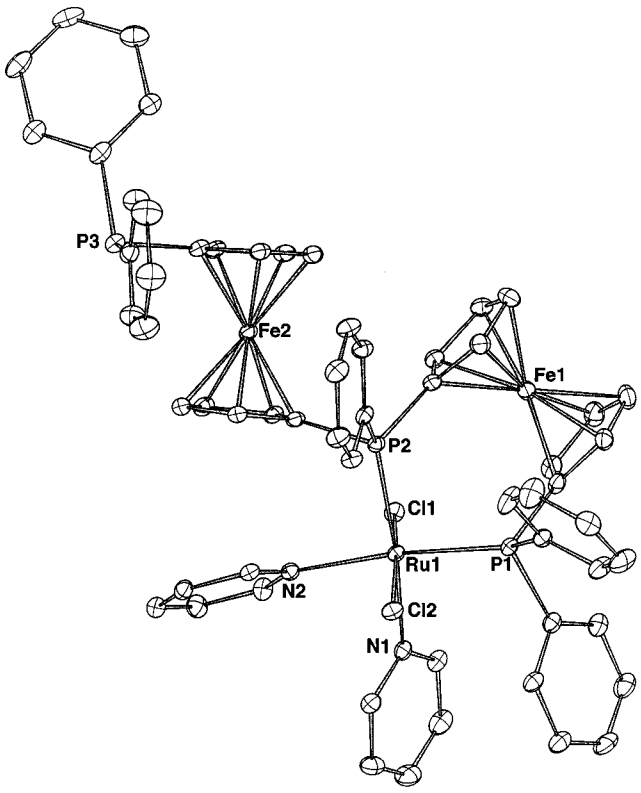

Fig. 4. Crystal structure of compound **5a**.

3.3. X-ray structure of $[P_2\text{-}(P_3\,fc)_2Ru(pyr)_2Cl_2]$ (**5a**)

The molecular structure and atomic labelling scheme of non-carbon atoms of **5a** are depicted in Fig. 4. To further increase the clarity of the figure the three acetone solvent molecules are omitted. Selected molecular geometry parameters are given in Table 2.

The structure of **5a** is comprised of a similar *PPP* ligand, with two ferrocenyl units, coordinated to an octahedral ruthenium centre as that of **3c** (vide supra). However in this instance the third phosphorus coordination site about the ruthenium has been displaced and is occupied by a pyridyl ligand, thus making the *PPP-2fc* ligand bidentate. The coordination environment of the Ru centre is very similar to that of **3c**, with the two chloride ligands trans to each other in axial positions and two phosphorus donors adjacent to each other in the equatorial plane but with the remaining two equatorial positions occupied by two pyridyl ligands as opposed to the third phosphorus and a carbonyl moiety. The coordination geometry is slightly distorted octahedral. This is much closer to idealised geometry than the complex **3c** (see angles about Ru(1) in Table 1), which is due to the greater strain on the coordination sphere imposed by binding the third chelate arm. The Ru–P distances are significantly shorter than those in **3c**, which is due to the reduced steric influence of a bidentate versus a tridentate ligand allowing donors to be closer, and hence bind more strongly, to the central metal acceptor. In addition the absence of other competing π-bonding ligands, such as the carbonyl group in **3c**, will cause a shortening of the phosphine–metal bond. The remaining bond lengths about the Ru centre are in accordance with those previously observed [11–17].

The geometric parameters observed for the coordinated part of the $\{Ph_2P(C_5H_4)_2Fe\}_2PPh$ ligand are similar to those previously observed in **3c**. The orientation of the ferrocenyl moiety involved in the chelate (Fe(1)) is very similar to that observed in **3c**, with Ru(1)–P(1)–C(23)–Fe(1) = 40.4(6)° and Ru(1)–P(2)–C(32)–Fe(1) = 19.6(5)° [41.3(9) and 19.6°, respectively, in **3c**]. This indicates a preferred orientation of the ferrocene group within this ligand when it bonds in a chelating mode. In contrast however, the pendant ferrocenyl donor arm (Fe(2)) has a torsion angle, Ru(1)–P(2)–C(39)–Fe(2) = 162.2(6)°, indicating complete freedom to adopt the most energetically favourable orientation. The angles about the uncoordinated phosphorus (P(3)) are all approximately 100°, which is typical of the pyramidal geometry adopted by free phosphines with relatively bulky functionality.

3.4. Electrochemistry

Figs. 5 and 6 summarize the changes in cyclic and differential pulse voltammetric responses recorded upon adding pyridine to dichloromethane solutions of complexes **2a** and **2b**, respectively.

Considering Fig. 5 initially, responses a, b, which show the electrochemical behaviour of **2a** before addition of pyridine, show two first reversible oxidations already discussed in a previous paper [2] which are assigned to the sequential one-electron oxidation of the two ferrocene subunits ($E' = +0.58$ V and $+0.85$ V, respectively). We now confidently assign the third most anodic step ($E^{\circ\prime} = +1.23$ V) to the Ru(II)/Ru(III) redox change, which is followed by chemical complications ($i_{pc}/i_{pa} = 0.6$ at 0.1 V s^{-1}). As deducible from responses c and d, a dramatic change takes place upon addition of pyridine. The Ru(II)/Ru(III) oxidation shifts by about 0.2 V towards less positive potential values ($E^{\circ\prime} = +1.02$ V). Concomitantly, the two ferrocene-centred oxidations tend to become irreversible. Taking into account that the diphenylphosphine-ligand, in the absence of the $RuCl_2$ coordination exhibits an irreversible two-electron oxidation, whereas in the presence of the ferrocenophane-type binding by $RuCl_2$ two reversible one-electron oxidations occur, we assign the behaviour of **2a** in the presence of pyridine to the release by the Ru(II) centre of one of the phosphino-cyclopentadienyl ligands, in agreement with the equilibrium shown in Scheme 2, which in the present case must clearly lie to the right.

In the case of complex **2b**, responses a, b parallel those discussed above with two first ferrocene-centred oxidations ($E^{\circ\prime} = +0.29$ and $+0.85$ V, respectively) followed by the Ru(II)/Ru(III) oxidation ($E^{\circ\prime} = +1.12$ V), complicated by following reactions ($i_{pc}/i_{pa} = 0.5$ at 0.1 V s^{-1}). As a consequence of the electron-donating ability of the ^{i}Pr phosphino-substituents, all the oxidation processes are easier than in complex **2a**. As responses c and d show, addition of pyridine slightly perturbs the voltammetric patterns. Essentially, the Ru(II)/Ru(III) oxidation splits into two parts, one of which is shifted towards more positive potential values by about 0.1 V ($E' = +1.03$ V). The two ferrocene oxidations maintain their features of chemical reversibility, with a very slight shift (because of the more emphasised roundness in DPV peaks), if any, towards more positive potential values. If an allowance is made

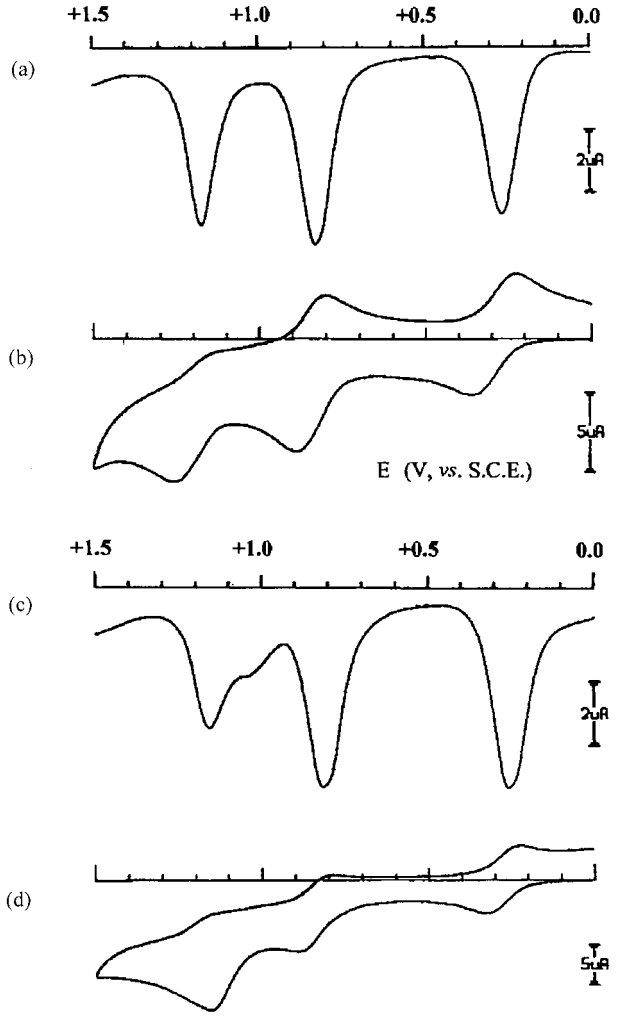

Fig. 5. Cyclic and differential pulse voltammograms recorded at a platinum electrode in CH_2Cl_2 solution containing compound **2a** (3.5×10^{-4} mol dm^{-3}) and NBu_4PF_6 (0.2 mol dm^{-3}). (a, b) Before addition of pyridine; (c, d) after addition of pyridine in about 1:2 (**17**:pyridine) ration. Scan rates: (a, c) 0.004 V s^{-1} (b, d) 0.1 V s^{-1}.

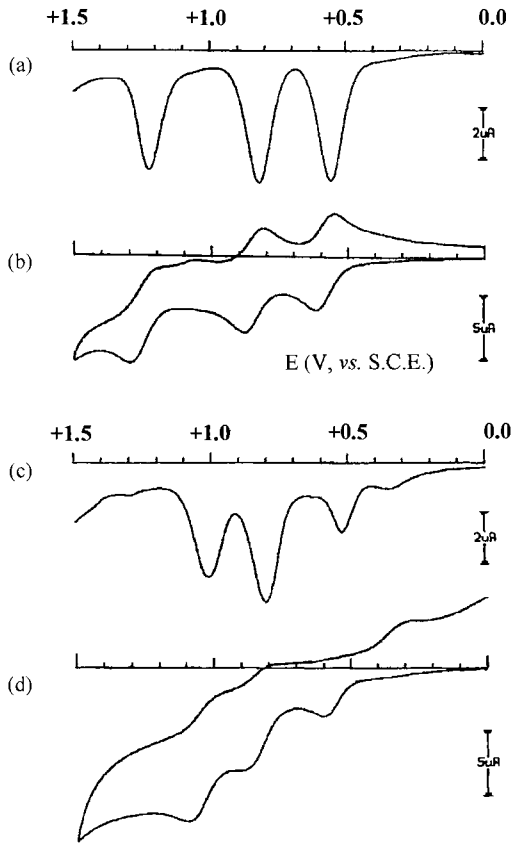

Fig. 6. Cyclic and differential pulse voltammograms recorded at platinum electrode in CH_2Cl_2 solution containing **2b** (4.5×10^{-4} mol dm^{-3}) and NBu_4PF_6 (0.2 mol dm^{-3}). (a, b) Before addition of pyridine; (c, d) after addition of pyridine in bout 1:2 (**2b**:pyridine) ratio. Scan rates: (a, c) 0.004 V s^{-1}; (b, d) 0.1 V s^{-1}.

to assign the partial shift of the Ru-centred oxidation to the pyridine coordination, the results show the equilibrium shown in Scheme 3 lies more to the left in this case.

In conclusion, electrochemical measurements indicate that the nature of the electron-donating groups in the phosphine ligands influences pyridine attachment to the ruthenium(II) centre, which is favoured by electron-withdrawing groups.

3.5. Molecular modelling

Molecular dynamics techniques have been used to study the influence of the addition of a second pyridine ligand on the conformation of the metal complexes **3a** and **3b**. Fig. 7 shows the conformation of the compound a as well as the conformation after addition of CO or pyridine. Geometry optimization was performed. A simple molecular modelling investigation was carried out on complexes **2a** and **3b**. The carbonyl complex **3c**, reported previously [2], was modelled and it was found that the geometry observed on the crystallographic study concurred with the minimum energy conformation predicted by the computer model (Fig. 7).

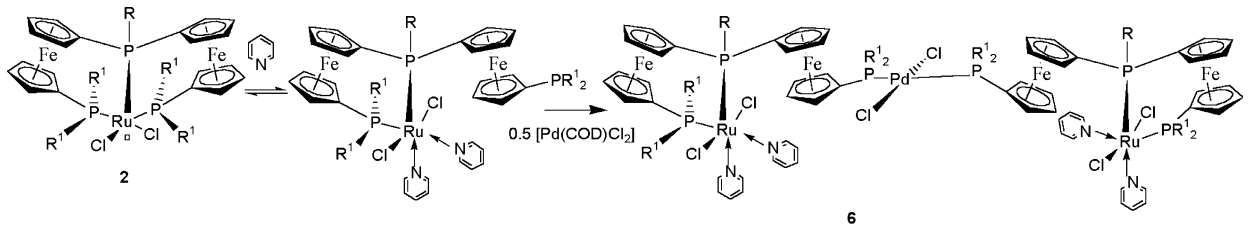

Scheme 2. Trapping the deligated phosphine with Pd(II).

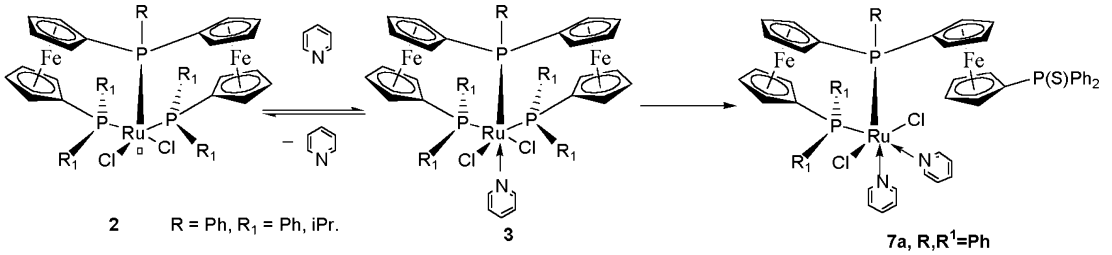

Scheme 3. Trapping the deligated phosphine with elemental sulfur.

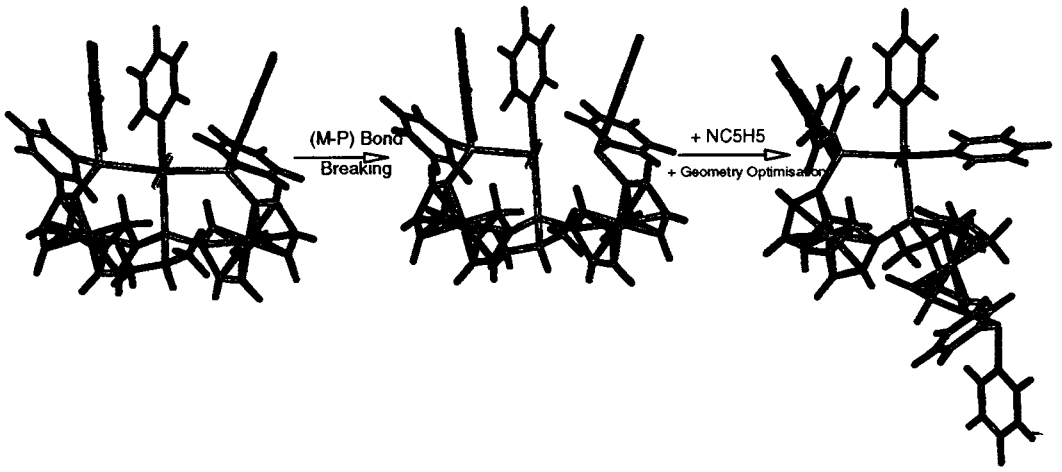

Fig. 7. The steric congestion is apparent on attempted pyridine coordination complex **2** and the deligation of a phosphine in complex **2a** showing the minimised conformation of complex **5a**.

Interestingly, when it was attempted simulate the binding of the pyridine to the five-coordinate complex it was clearly obvious that, due to the steric crowding, the six-coordinate complex was unstable. If a phosphine was deligated the pyridine was able to bind readily and indeed it was possible to coordinate a second pyridine. It became clear that before deligation takes place, a minimum concentration of pyridine in solution is required, i.e. equilibrium according to Scheme 1 exists between the pyridine and the deligated complex. However no intermediate was detected using NMR, although both products **5** and the starting complex **2** may be observed in solution simultaneously.

In conclusion the reaction chemistry of these ruthenium complexes is non-trivial: the reaction chemistry is dependent on the nature of the incoming ligand. With non-sterically demanding π-acceptor ligands the vacant sixth coordination site is filled, while with weaker field ligands partial deligation of one of the phosphines is also observed. Finally non-sterically demanding π-donor ligands lead to only an equilibrium where phosphine deligation is observed. Clearly the coordination chemistry should be further studied with other substrates and its catalytic reactions should investigated be a matter of priority. The electrochemical results also indicate the importance of the nature of the phosphine ligands in solution equilibria. These studies will be the subject of the next paper in the series.

4. Supplementary material

Crystallographic data for the structural analysis have been deposited with the Cambridge Crystallographic

Data Centre, CCDC Nos. 154080 for **3c** and 154081 for **5b**. Copies of this information may be obtained free of charge from The Director, CCDC, 12 Union Road, Cambridge CB2 1EZ, UK (fax: +44-1233-336033; e-mail: deposit@ccdc.cam.ac.uk or www: http://www.ccdc.cam.ac.uk).

Acknowledgements

IRB gratefully acknowledges the support of the University of Wales for sponsoring this research. Mass spectroscopic data were obtained at the University of Wales, Swansea, central EPSRC service whose aid we gratefully acknowledge. PZ gratefully acknowledges the financial support of the University of Siena (PAR 1999). A range of supporting data and figures may be obtained on request (authors@ferrocene.com).

References

[1] I.R. Butler, R.L. Davies, Synthesis (1996) 1350.
[2] I.R. Butler, U. Griesbach, P. Zanello, D.E. Hibbs, M.B. Hursthouse, K.M.A. Malik, J. Organomet. Chem. 565 (1998) 243.
[3] (a) M.M. Taquikhan, R. Mohiuddina, J. Coord. Chem. 6 (1977) 171;
(b) C. Bianchini, P.J. Perez, M. Peruzzini, F. Zanobini Avacca, Inorg. Chem. 30 (1991) 279.
[4] J.A. Darr, S.R. Drake, M.B. Hursthouse, K.M.A. Malik, Inorg. Chem. 32 (1993) 5704.
[5] N.P.C. Walker, D. Stuart, DIFABS Program for Absorption Correction, Acta Crystallogr. Sect. A 39 (1983) 158; adapted for FAST geometry by A.I. Karaulov, University of Wales Cardiff, 1991.
[6] G.M. Sheldrick, SHELXS-86, Program for Crystal Structure Solution, Acta Crystallogr. Sect. A 46 (1990) 467.
[7] G.M. Sheldrick, SHELXL-93, Program for Crystal Structure Refinement, University of Göttingen, Germany, 1993.
[8] R. Hooft, B.V. Nonius, COLLECT: data collection software, 1998.
[9] R.H. Blessing, J. Appl. Crystallogr. 30 (1997) 421.
[10] G.M. Sheldrick, SHELXL-97, Program for Crystal Structure Solution and Refinement, University of Gottingen, Germany, 1997.
[11] A. Albinati, Q. Zhong Jiang, H. Ruegger, L.M. Venanzi, Inorg. Chem. 32 (1993) 4940.
[12] R.R. Guimerans, E.C. Hernandez, M.M. Olmstead, A.L. Balch, Inorg. Chim. Acta 165 (1989) 45.
[13] G. Delgado, A.V. Rivera, T. Suarez, B. Fontal, Inorg. Chim. Acta 233 (1995) 145.
[14] L. Solujic, E.B. Milosavijevic, J.H. Nelson, N.W. Alcock, J. Fischer, Inorg. Chem. 28 (1989) 3453.
[15] W.S. Sheldrick, K. Brandt, Inorg. Chim. Acta 217 (1994) 51.
[16] G. Jia, I. Lee, D.W. Meek, J.C. Gallucci, Inorg. Chim. Acta 177 (1990) 81.
[17] I. Dahlenburg, S. Kerstan, D. Werner, J. Organomet. Chem. 411 (1991) 457.
[18] K. Davies, SNOOPI, Program for Crystal Structure Drawing, University of Oxford, UK, 1983.